

# A unified model for simulating liquid and gas phase, intermolecular energy transfer: $\text{N}_2$ + $\text{C}_6\text{F}_6$ collisions

Amit K. Paul, Swapnil C. Kohale, Subha Pratihari, Rui Sun, Simon W. North, and William L. Hase'

Citation: *J. Chem. Phys.* **140**, 194103 (2014); doi: 10.1063/1.4875516

View online: <http://dx.doi.org/10.1063/1.4875516>

View Table of Contents: <http://aip.scitation.org/toc/jcp/140/19>

Published by the [American Institute of Physics](#)

---

---

# A unified model for simulating liquid and gas phase, intermolecular energy transfer: $\text{N}_2 + \text{C}_6\text{F}_6$ collisions

Amit K. Paul,<sup>1</sup> Swapnil C. Kohale,<sup>1</sup> Subha Pratihar,<sup>1</sup> Rui Sun,<sup>1</sup> Simon W. North,<sup>2</sup> and William L. Hase<sup>1,a)</sup>

<sup>1</sup>Department of Chemistry and Biochemistry, Texas Tech University, Lubbock, Texas 79409, USA

<sup>2</sup>Department of Chemistry, Texas A&M University, College Station, Texas 77842, USA

(Received 2 January 2014; accepted 28 April 2014; published online 20 May 2014)

Molecular dynamics simulations were used to study relaxation of a vibrationally excited  $\text{C}_6\text{F}_6^*$  molecule in a  $\text{N}_2$  bath. *Ab initio* calculations were performed to develop  $\text{N}_2\text{-N}_2$  and  $\text{N}_2\text{-C}_6\text{F}_6$  intermolecular potentials for the simulations. Energy transfer from “hot”  $\text{C}_6\text{F}_6$  is studied versus the bath density (pressure) and number of bath molecules. For the large bath limit, there is no heating of the bath. As  $\text{C}_6\text{F}_6^*$  is relaxed, the average energy of  $\text{C}_6\text{F}_6^*$  is determined versus time, i.e.,  $\langle E(t) \rangle$ , and for each bath density  $\langle E(t) \rangle$  is energy dependent and cannot be fit by a single exponential. In the long-time limit  $\text{C}_6\text{F}_6$  is fully equilibrated with the bath. For a large bath and low pressures, the simulations are in the fixed temperature, independent collision regime and the simulation results may be compared with gas phase experiments of collisional energy transfer. The derivative  $d[\langle E(t) \rangle]/dt$  divided by the collision frequency  $\omega$  of the  $\text{N}_2$  bath gives the average energy transferred from  $\text{C}_6\text{F}_6^*$  per collision  $\langle \Delta E_c \rangle$ , which is in excellent agreement with experiment. For the  $\sim 100\text{--}300$  ps simulations reported here, energy transfer from  $\text{C}_6\text{F}_6^*$  is to  $\text{N}_2$  rotation and translation in accord with the equipartition model, with no energy transfer to  $\text{N}_2$  vibration. The energy transfer dynamics from  $\text{C}_6\text{F}_6^*$  is not statistically sensitive to fine details of the  $\text{N}_2\text{-C}_6\text{F}_6$  intermolecular potential. Tests, with simulation ensembles of different sizes, show that a relatively modest ensemble of only 24 trajectories gives statistically meaningful results. © 2014 AIP Publishing LLC. [<http://dx.doi.org/10.1063/1.4875516>]

## I. INTRODUCTION

The study of collisional intermolecular energy transfer (IET) of highly vibrationally excited molecules to thermalized bath molecules has received considerable investigation.<sup>1–6</sup> In pyrolysis, combustion, and atmospheric chemistry highly vibrationally excited molecules play an important role and a detailed understanding of their relaxation processes is truly desirable. Theoretically, the most familiar way to investigate IET is based on a master equation calculation in terms of the energy transfer rate coefficient  $R(E,E')$  or the energy transfer probability distribution function  $P(E,E')$ .<sup>4</sup> Once obtained,<sup>7,8</sup>  $P(E,E')$  may be used to calculate an average  $\Delta E$  per collision. Another model called the *Biased Random Walk*<sup>9</sup> has often been used to obtain  $\Delta E$  quantities from the results of a few trajectories.

In a series of exploratory studies, classical trajectory simulations were used to investigate how potential energy surface (PES) properties and collision attributes affect IET.<sup>10–13</sup> Theoretical analyses of IET have considered the excited molecules  $\text{HO}_2$ ,<sup>14</sup>  $\text{CS}_2$ ,<sup>15–17</sup>  $\text{H}_2\text{O}$ ,<sup>18</sup>  $\text{SO}_2$ ,<sup>17</sup> benzene,<sup>8,19–23</sup> *p*-difluorobenzene,<sup>23</sup> toluene,<sup>24,25</sup> hexafluorobenzene,<sup>19,20</sup> and azulene,<sup>26–31</sup> colliding with either a monoatomic or polyatomic bath gas. A number of experimental techniques have been used to measure collisional energy transfer quantities. Barker *et al.* used an infrared fluorescence de-

tection technique,<sup>32–38</sup> for vibrationally excited hydrocarbons like azulene,<sup>32</sup> benzene,<sup>33,34,36,37</sup> and toluene.<sup>34,35,37</sup> Mullin *et al.* have applied<sup>39–49</sup> high resolution infrared laser transient absorption spectroscopy to study energy transfer from pyrazine,<sup>39,42–46,49</sup> pyridine,<sup>41,48</sup> hexafluorobenzene,<sup>40</sup> and azulene.<sup>47</sup> Flynn studied relaxation of benzene,<sup>50</sup> benzene-*d*6,<sup>50</sup> hexafluorobenzene,<sup>50,51</sup> and pyrazine<sup>51</sup> in collisions with  $\text{CO}_2$  using time resolved diode laser spectroscopy. Isomers of difluorobenzene in collisions with  $\text{CO}_2$  have also been studied using the same technique.<sup>52</sup> Troe *et al.* followed the collisional relaxation of several hot molecules<sup>53,54</sup> using time-resolved UV absorption spectroscopy.<sup>55</sup> The same time-resolved UV absorption spectroscopy was used for studying collisional relaxation of benzene<sup>56</sup> and hexafluorobenzene.<sup>57–59</sup> Recently, Ni *et al.* have used a molecular beam apparatus with a time-sliced velocity map ion imaging technique to study collisional energy transfer from azulene,<sup>60</sup> and naphthalene<sup>61–64</sup> and its derivatives,<sup>65</sup> in collisions with monoatomic<sup>60–63,65</sup> as well as polyatomic<sup>64</sup> bath gases. Several other experimental techniques have also been used, namely, kinetically controlled selective ionization (KCSI) detection,<sup>66,67</sup> infrared multiphoton absorption (IRMPA) coupled with time resolved infrared fluorescence (IRF),<sup>68–70</sup> and supersonic free jet expansion.<sup>71,72</sup>

Simulations based on accurate intermolecular potentials between the excited molecule and the bath gas, and between the bath gases, may be used to obtain accurate IET dynamics and make rigorous comparisons with experiment.<sup>15,16</sup> Also of interest are simulations which investigate the role

<sup>a)</sup> Author to whom the correspondence should be addressed. Electronic mail: bill.hase@ttu.edu

of the bath density (pressure) on energy transfer processes for the hot molecule. Of interest is how the dynamics of energy transfer from the excited molecule change in going from the condensed to gas phase. Properties of vibrational relaxation of highly excited molecules have been studied in fluids<sup>31,73,74</sup> and a few recent calculations have been done at various densities.<sup>75–79</sup> However, this work<sup>75–79</sup> was performed to only consider efficient approaches for low density simulations.

In the work presented here a unified chemical dynamics simulation approach is used to study  $C_6F_6^* + N_2$  IET in both the gas and liquid phases. The simulations are performed with a vibrationally excited  $C_6F_6^*$  molecule in a bath of  $N_2$  molecules at different densities and at an initial temperature of 298 K. Related many-atom simulations have been performed by Schwartzenuber and co-workers.<sup>77,78</sup> As the density is lowered, the system enters the single collision regime and an analysis of the simulations gives results that may be compared directly with gas-phase experiments of IET. The standard simulation approach is to calculate trajectories for a fixed vibrational energy  $E$  and collision translational energy versus impact parameter, for random orientations of the collision partners.<sup>10–16</sup> For the current study the averaging over impact parameter and orientations is accomplished by simulating the vibrationally excited molecule in a “bath” of deactivating molecules.

The remainder of this article is organized as follows. The intermolecular potentials for  $N_2$ - $N_2$  and  $C_6F_6$ - $N_2$ , used in the simulations are calculated at the MP2 level of theory, with an optimum cost-effective basis set, and these potentials and their fittings are discussed in Sec. II. Details of the chemical dynamics simulation methodology and analyses of the simulation results are presented in Sec. III. The simulation results and their discussion is given in Sec. IV. The article concludes with a summary in Sec. V.

## II. POTENTIAL

The potential energy function for the  $C_6F_6 + N_2$ -bath system is written as the sum

$$V = V_{C_6F_6} + V_{N_2} + V_{N_2, C_6F_6} + V_{N_2, N_2}, \quad (1)$$

where  $V_{C_6F_6}$  and  $V_{N_2}$  are the intramolecular potentials, and  $V_{N_2, C_6F_6}$  and  $V_{N_2, N_2}$  are the  $C_6F_6$ - $N_2$  and  $N_2$ - $N_2$  intermolecular potentials. Each of these potentials is described in the following.

### A. Intramolecular potentials

The intramolecular potential used for hexafluorobenzene (HFB) is expressed in internal stretching and bending coordinates, with force constants that give HFB vibrational frequencies in very good agreement with the experiment.<sup>20</sup> The functional form used for this potential is the same as that used previously<sup>20</sup> except the Morse stretching potential,  $V(R) = D_e(1 - e^{-\beta_e(R-R_e)})$ , was used for the C–C and C–F bonds instead of the harmonic stretch potential.  $D_e$  and  $R_e$  for the C–C and C–F bonds of HFB are 124 kcal/mol (as for benzene C–C bonds)<sup>80</sup> and 1.394 Å,<sup>20</sup> and 116 kcal/mol,<sup>81</sup> and

1.327 Å,<sup>20</sup> respectively. The respective values of  $\beta_e$  for the C–C and C–F bonds are 1.83 and 2.03 Å<sup>-1</sup>, and calculated from the stretching force constants using  $\beta_e = (f/2D_e)^{1/2}$ . For  $N_2$ , the parameters are taken as  $D_e = 228.3$  kcal/mol,  $\beta_e = 2.699$  Å<sup>-1</sup>, and  $R_e = 1.0945$  Å.<sup>82</sup>

### B. Intermolecular potentials

Electronic structure calculations for the  $N_2$ - $N_2$  and  $N_2$ - $C_6F_6$  intermolecular potentials were performed with the NWChem quantum chemistry package.<sup>83</sup> MP2 theory,<sup>84</sup> with the frozen-core approximation, is used for the calculations. Energies are computed with and without a basis set superposition error (BSSE) correction.<sup>85</sup> Previous work has shown that MP2 with the moderate basis set aug-cc-pVTZ gives energies comparable to CCSD(T) for the complete basis set (CBS) limit.<sup>86–88</sup>

#### 1. $N_2$ - $N_2$ potential

In previous work,<sup>89,90</sup> detailed analytic potentials have been developed for the  $N_2$ - $N_2$  intermolecular interaction. For the molecular dynamics simulations performed here a less complicated potential, written as a sum of two-body terms, is desirable. Thus, to develop an analytic potential, the  $N_2$ - $N_2$  intermolecular interaction was calculated for the three different orientations in Figure 1 using MP2 and the three basis sets aug-cc-pVDZ, aug-cc-pVTZ, and aug-cc-pVQZ. For each orientation, the calculations for the three basis sets are extrapolated to the CBS limit using the formula<sup>91</sup> and the minimum energy potential energy for each basis set; i.e.,

$$E(n) = E_{CBS} + A \exp[-(n-1)] + B \exp[-(n-1)^2], \quad (2)$$

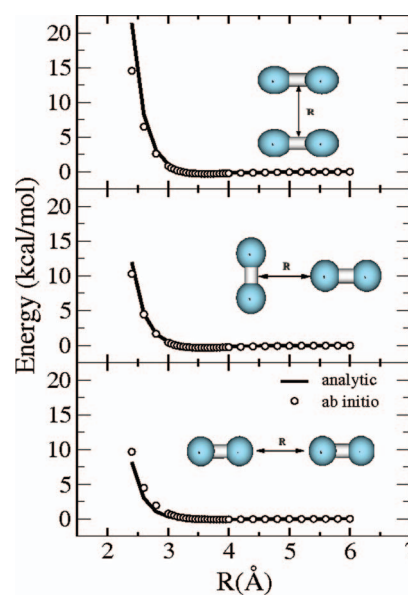


FIG. 1.  $N_2$ - $N_2$  interaction potential energy for three different orientations. The *ab initio* curves are calculated at the MP2/aug-cc-pVTZ level of theory, whereas the analytic curves are generated by fitting the *ab initio* potential to the two-body potentials in Eq. (4) with the parameters listed in Table II.

TABLE I. MP2 potential energy minima with different basis sets for three different N<sub>2</sub>-N<sub>2</sub> orientations.<sup>a</sup>

| BSSE <sup>b</sup> | aug-cc-pVDZ    |                | aug-cc-pVTZ    |                | aug-cc-pVQZ    |                | CBS            |
|-------------------|----------------|----------------|----------------|----------------|----------------|----------------|----------------|
|                   | R <sub>0</sub> | V <sub>0</sub> | R <sub>0</sub> | V <sub>0</sub> | R <sub>0</sub> | V <sub>0</sub> | V <sub>0</sub> |
| Parallel          |                |                |                |                |                |                |                |
| No corr           | 3.58           | -0.54          | 3.51           | -0.49          | 3.56           | -0.41          | -0.36          |
| Corr              | 3.69           | -0.27          | 3.62           | -0.32          | 3.60           | -0.33          | -0.34          |
| Perpendicular     |                |                |                |                |                |                |                |
| No corr           | 3.48           | -0.55          | 3.45           | -0.52          | 3.47           | -0.44          | -0.39          |
| Corr              | 3.62           | -0.22          | 3.58           | -0.34          | 3.53           | -0.35          | -0.35          |
| Linear            |                |                |                |                |                |                |                |
| No corr           | 3.61           | -0.29          | 3.61           | -0.25          | 3.67           | -0.16          | -0.10          |
| Corr              | 3.84           | -0.09          | 3.81           | -0.09          | 3.79           | -0.09          | -0.09          |

<sup>a</sup>Values of R<sub>0</sub> and V<sub>0</sub> are listed in Å and kcal/mol, respectively.

<sup>b</sup>Calculations are with and without a BSSE correction.

where  $n$  is the cardinal number of the basis set. The results are presented in Table I. For MP2 theory, CBS intermolecular energies are expected to be less accurate than those obtained with the aug-cc-pVTZ basis set.<sup>86,87</sup>

The three N<sub>2</sub>-N<sub>2</sub> intermolecular potential energy curves calculated with MP2/ aug-cc-pVTZ (Figure 1) were used to develop an analytic N<sub>2</sub>-N<sub>2</sub> intermolecular potential. This latter potential is written as a sum of two-body interactions between the N-atoms of the two molecules and the parameters for these interactions were determined by simultaneously fitting the three MP2 potential energy curves using a genetic algorithm.<sup>92</sup> A modified Buckingham two-body potential of the form

$$V = A \exp(-Br) + \frac{C}{r^n} + \frac{D}{r^m} \quad (3)$$

gave accurate fits to *ab initio* potential energy curves in previous work,<sup>87,88,93</sup> but it did not give a good fit for three N<sub>2</sub>-N<sub>2</sub> potential energy curves. To add more flexibility to Eq. (3), the following two-body potential was used for the fitting:

$$V = A \exp[-B(r + b)] + \frac{C}{(r + c)^n} + \frac{D}{(r + d)^m} \quad (4)$$

allowing  $b$ ,  $c$ , and  $d$  to take any value from negative to positive. With this function an overall good fit to the MP2/aug-cc-pVTZ potential curves was obtained as shown in Figure 1. The fitted parameters are listed in Table II. The MP2 V<sub>0</sub>, R<sub>0</sub> values for the top curve (parallel orientation) and middle curve (perpendicular orientation) in Figure 1 are -0.32 kcal/mol, 3.62 Å and -0.34 kcal/mol, 3.58 Å, re-

spectively. The respective V<sub>0</sub>, R<sub>0</sub> values for the fitted curves are -0.19 kcal/mol, 3.80 Å and -0.14 kcal/mol, 3.70 Å. For the bottom curve (linear orientation), the interaction is purely repulsive. The repulsive regions of the potential energy curves are fit quite well for energies corresponding to those for a N<sub>2</sub> bath at 298 K, for which the average N<sub>2</sub> + N<sub>2</sub> collision energy is ~0.9 kcal/mol

## 2. N<sub>2</sub>-C<sub>6</sub>F<sub>6</sub> potential

Because of the “electronic” size of the N<sub>2</sub>-C<sub>6</sub>F<sub>6</sub> system, it is of interest to determine if a smaller molecular system may be used to model the N<sub>2</sub>-C<sub>6</sub>F<sub>6</sub> intermolecular interaction. The C-atom hybridization for C<sub>6</sub>F<sub>6</sub> is sp<sup>2</sup> and the same as that for C<sub>2</sub>F<sub>4</sub>, however the C-C bond order for C<sub>6</sub>F<sub>6</sub> is smaller. As a “test” of this latter difference, intermolecular potentials were calculated and compared for a Ne-atom interacting with CF<sub>4</sub> and C<sub>2</sub>F<sub>4</sub>. Potential energy curves were calculated for the Ne-atom: (1) approaching the C-atom of CF<sub>4</sub> backside along a C-F bond axis and approaching a C-atom of C<sub>2</sub>F<sub>4</sub> perpendicular to the plane of C<sub>2</sub>F<sub>4</sub>, i.e., Ne-C curves; and (2) approaching a F-atom directly along the C-F bond of CF<sub>4</sub> and C<sub>2</sub>F<sub>4</sub>, i.e., Ne-F curves. For the Ne-C curves V<sub>0</sub>, R<sub>0</sub> are -0.152 kcal/mol, 3.52 Å and -0.190 kcal/mol, 3.43 Å for CF<sub>4</sub> and C<sub>2</sub>F<sub>4</sub>, respectively. For the Ne-F curves the respective V<sub>0</sub>, R<sub>0</sub> are -0.103 kcal/mol, 3.12 Å and -0.109 kcal/mol, 3.11 Å. The differences between the interaction energies of Ne to CF<sub>4</sub> and C<sub>2</sub>F<sub>4</sub> are small, indicating that C<sub>2</sub>F<sub>4</sub> may be used to model C<sub>6</sub>F<sub>6</sub> in the N<sub>2</sub>-C<sub>6</sub>F<sub>6</sub> intermolecular potential without a substantial loss of accuracy.

For an initial determination of the N<sub>2</sub>-C<sub>6</sub>F<sub>6</sub> intermolecular potential, MP2/aug-cc-pVTZ potential energy curves were calculated for the three orientations shown in Figure 2. An excellent fit to these curves is obtained with a sum of F-N and C-N two-body potentials given by Eq. (3) and the fitted parameters are given in Table II for PES1. The MP2 V<sub>0</sub> (kcal/mol), R<sub>0</sub> (Å) values for the top, middle, and bottom curves are -1.04, 3.28, -0.27, 3.21, and -0.95, 3.37, respectively. In comparison, the fitted curves give respective values of -1.07, 3.31, -0.19, 3.20, and -1.12, 3.33. Overall, the fit to these three curves is quite good for PES1.

A test of the PES1 analytic potential energy function was made using MP2/aug-cc-pVTZ to calculate the potential energy curve for the bottom orientation in Figure 3, which was compared with the potential energy curve given for this orientation by PES1. The MP2 V<sub>0</sub> (kcal/mol), R<sub>0</sub> (Å) values are -0.72, 3.48, in comparison to -1.60, 3.40 for PES1. The difference in V<sub>0</sub> is substantial and 0.88 kcal/mol. Thus, though

TABLE II. Parameters for the N<sub>2</sub>-N<sub>2</sub> and N<sub>2</sub>-C<sub>6</sub>F<sub>6</sub> intermolecular potentials fit to MP2/aug-cc-pVTZ calculations.<sup>a</sup>

| Interaction             | A        | B        | b          | C         | c          | D        | d          | n | m   |
|-------------------------|----------|----------|------------|-----------|------------|----------|------------|---|-----|
| N-N <sup>b</sup>        | 13454.28 | 4.514701 | 0.02306411 | -214.8792 | -0.5683582 | 11305.30 | -0.2905575 | 6 | 9   |
| C-N (PES1) <sup>c</sup> | 45854.13 | 3.199410 | ...        | -6702.036 | ...        | ...      | ...        | 7 | ... |
| C-N (PES2) <sup>b</sup> | 99569.69 | 4.495995 | -0.2239541 | -51703.28 | 2.696324   | 99087.81 | 0.8693999  | 7 | 10  |
| F-N (PES1) <sup>c</sup> | 212209.9 | 4.668711 | ...        | -54.90112 | ...        | 1067.110 | ...        | 7 | 10  |
| F-N (PES2) <sup>b</sup> | 854509.8 | 4.212151 | 0.5417893  | -19432.07 | 3.931211   | 78636.53 | 3.078181   | 6 | 9   |

<sup>a</sup>Units of the parameters are A in kcal/mol, B in Å<sup>-1</sup>, C in kcal Å<sup>n</sup>/mol, c in Å, D in kcal Å<sup>m</sup>/mol, d in Å.

<sup>b</sup>Fit with Eq. (4).

<sup>c</sup>Fit with Eq. (3).

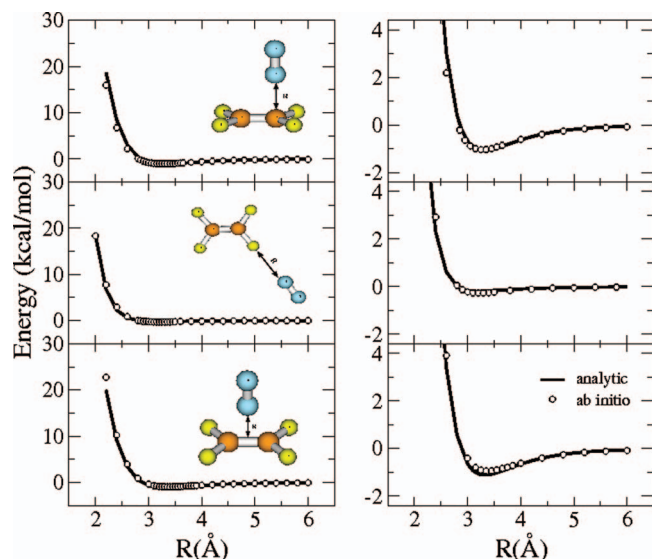


FIG. 2.  $C_2F_4-N_2$  interaction potential energy for three different orientations. The *ab initio* curves are calculated at the MP2/aug-cc-pVTZ level of theory, whereas the analytic curves are generated by fitting the *ab initio* potential to the two-body potentials in Eq. (3) with the parameters listed in Table II for PES1. The right-hand side panels are for lower energies in the potential energy curves and fit by PES1.

PES1 fits the three potential energy curves in Figure 2, it does not fit this latter potential energy curve.

A quite good fit to all four potential energy curves in Figure 3 is found with a sum of the two-body potentials in Eq. (3), but an even better fit is obtained using Eq. (4) for the two-body potentials. The parameters are listed in Table II and identified as PES2. The fit is illustrated in Figure 3. As shown below in Sec. IV D, PES1 and this more accurate PES2 give statistically the same  $N_2 + C_6F_6$  intermolecular energy transfer dynamics.

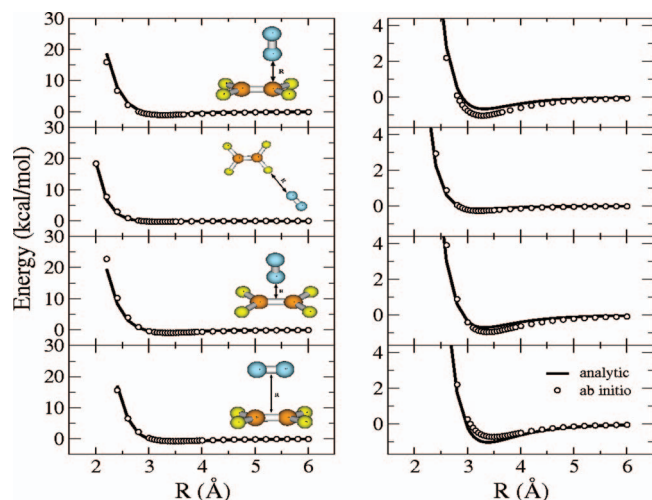


FIG. 3.  $C_2F_4-N_2$  interaction potential energy for four different orientations. The *ab initio* curves are calculated at the MP2/aug-cc-pVTZ level of theory, whereas the analytic curves are generated by fitting the *ab initio* potential to the two-body potentials in Eq. (4) with the parameters listed in Table II for PES2. The right-hand side panels are for lower energies in the potential energy curves and fit by PES2.

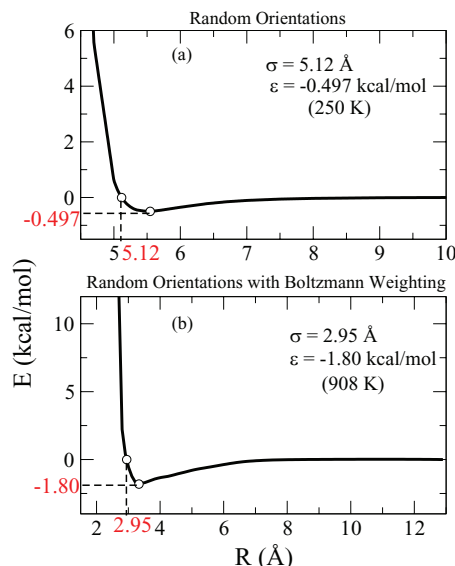


FIG. 4. Angle averaged  $C_6F_6-N_2$  interaction potential for the PES2 two-body potential in Table II.  $R$  is the  $C_6F_6 + N_2$  center-of-mass separation. For the top curve (a) both  $C_6F_6$  and  $N_2$  are randomly rotated about their Euler angles. For the bottom curve (b) each random orientation is Boltzmann weighted by the orientation's  $C_6F_6-N_2$  intermolecular potential.

To determine the collisional energy transfer efficiency, a standard approach is to represent the intermolecular potential between the collision partners by an “average” Lennard-Jones potential.<sup>8</sup> An average interaction between  $N_2$  and  $C_6F_6$  was calculated as a function of their center of mass separation between 2 and 13 Å. Two approaches were used to determine this average  $N_2 + C_6F_6$  interaction potential. For one, an average potential was calculated for each separation by averaging over random orientations of  $N_2$  and  $C_6F_6$ ,<sup>94</sup> without any weighting of the interaction potential energy. The resulting potential using the PES2 parameters is shown in Figure 4(a). The respective Lennard-Jones parameters for  $\sigma$  and  $\epsilon$  are 5.12 Å and 250 K (−0.497 kcal/mol). For comparison, PES1 gives these parameters as 5.07 Å and 282 K (−0.560 kcal/mol), for this averaging. Though the simulations are not performed under equilibrium conditions, for comparison with the above potential an interaction potential was calculated by weighting each random orientation by the Boltzmann term  $\exp[-V(\text{orient})/k_B T]$  for its potential  $V(\text{orient})$ .<sup>95</sup> This weighting emphasizes the most attractive  $N_2 + C_6F_6$  interactions and its potential energy curve is given in Figure 4(b) for PES2; the  $\sigma$  and  $\epsilon$  parameters are 2.95 Å and 908 K (−1.80 kcal/mol). The curve in Figure 4(a), without this Boltzmann weighting, is based on an approach similar to that used by Bernshtein and Oref for  $Ar + C_6H_6$ .<sup>8</sup>

### III. SIMULATION METHODOLOGY

#### A. Initial conditions for $C_6F_6$ , and solvent preparation

The experiments modeled in these simulations are those in which HFB is electronically excited to  $S_1$  with 266 nm excitation and then undergoes a radiationless transition to  $S_0$ , preparing “hot” HFB with 107.4 kcal/mol vibrational energy.<sup>40</sup> For the trajectory initial conditions, this energy was

added to HFB using classical microcanonical normal mode sampling<sup>96</sup> as implemented in the VENUS chemical dynamics package.<sup>97</sup> The initial translational and rotational energies of HFB are chosen from their thermal distributions at 298 K.

Energy transfer from this excited HFB molecule is studied in the presence of a “bath” of N<sub>2</sub> molecules. Because of the weak coupling of N<sub>2</sub> vibration with N<sub>2</sub> rotation and translation, the dynamics of the bath is not ergodic on the time scale of a standard molecular dynamics (MD) simulation.<sup>98</sup> Such a simulation, with scaling of the velocities to attain the desired temperature, will not give an equilibrium distribution. Thus, the following scheme was used to fully equilibrate the bath. The sampling begins by placing the N<sub>2</sub> molecules uniformly in a cubic box with periodic boundary conditions and placing the HFB molecule, with its initial conditions, in the middle of the box. The box size is determined by the number of N<sub>2</sub> molecules and the bath density (see below). The Boltzmann probability distribution of the N<sub>2</sub> potential energy

$$P(\Delta r) \propto \exp(-k\Delta r^2/2k_B T) \quad (5)$$

is sampled for each N<sub>2</sub> molecule to determine its bond length; i.e., here  $k$  is the force constant, and  $\Delta r$  is the displacement of the bond from equilibrium. The average N<sub>2</sub> potential energy resulting from this sampling is  $k_B T/2$ . The one-dimensional velocity distribution is then sampled for  $v_x$ ,  $v_y$ , and  $v_z$  of each N-atom of the N<sub>2</sub> bath. This sampling adds on average, to the N<sub>2</sub> bath molecules,  $3k_B T/2$  to center of mass translation,  $k_B T$  to rotation, and  $k_B T/2$  to vibrational kinetic energy.

A MD simulation<sup>98</sup> is then performed for the N<sub>2</sub> solvent system for approximately 90 ps in a stagewise manner and with HFB fixed with its initial conditions in the middle of a cubic box. Since HFB is kept rigid for this equilibration, the potential energy is  $V_{N_2} + V_{N_2, C_6F_6} + V_{N_2, N_2}$ ; see Eq. (1). The coordinates and velocities of HFB are not altered during the equilibration. Each stage of the equilibration is divided into two parts – sampling and monitoring. For the sampling part, the trajectory is calculated with 2000 integration steps and the  $v_x$ ,  $v_y$ , and  $v_z$  components of the N-atom velocities were re-sampled every 5 integration steps. For the monitoring part of this trajectory, also integrated with 2000 steps, the velocities of the N-atoms are not re-sampled and energy conservation is important. The properties of the solvent bath monitored in the second part are its temperature, radial distribution function,<sup>99</sup> and vibrational, rotational, and center-of-mass translational energies. The final configuration of the solvent molecules at the end of each stage of the equilibration is saved and the next stage is started from that configuration with a larger integration step size ( $\Delta t$ ). The step size is increased in this manner as long as the total energy of the solvent is conserved during the monitoring part of the equilibration. The larger step size provides an equilibration stage with a longer total integration time. The same step size is used to calculate the trajectories for C<sub>6</sub>F<sub>6</sub> energy transfer to the N<sub>2</sub> bath. The temperature of the N<sub>2</sub> bath is determined from

$$3LRT/2 = \sum_i \frac{mv_i^2}{2}, \quad (6)$$

where  $L$  is the number of N atoms,  $R$  is the gas law constant,  $m$  is the mass of a N atom,  $v_i$  is the velocity of the  $i$ th N atom, and the summation on the rhs extends from  $i = 1$  to  $L$ .

Thermal equilibration of N<sub>2</sub> solvent is completed when the average temperature of the solvent is 298 K and the solvent has a proper radial distribution function.<sup>99</sup> The temperature was found to converge quite rapidly, but more equilibration steps were required to converge the radial distribution function. The resulting initial condition for the bath had a 298 K temperature, the correct radial distribution function, and the correct average thermal translational, rotational, and vibrational energies of  $3k_B T/2$ ,  $k_B T$ , and  $k_B T$ , respectively, for the N<sub>2</sub> molecules.

For each simulation an ensemble of trajectories was calculated with random initial conditions. The initial conditions for the first trajectory in the ensemble were chosen as described above. For the remaining trajectories HFB had random initial conditions as specified by the microcanonical ensemble. To select random initial conditions for the solvent molecules the following procedure was used. After equilibration of the first trajectory in the ensemble (see above) it was integrated for an additional 6 ps period of time and up to 8 sets of configurations and velocities for the solvent were saved at random time intervals. Each of these configurations was used to select solvent initial conditions for trajectories in groups of 12. The initial conditions for each of these trajectories were further randomized by holding HFB rigid and equilibrating the N<sub>2</sub> bath for 12 ps. Thus, each trajectory in the ensemble had random initial conditions for HFB and the N<sub>2</sub> bath.

The heating of the N<sub>2</sub> solvent as energy is transferred from “hot” HFB depends on the number of N<sub>2</sub> molecules, i.e., the relative HFB and N<sub>2</sub> densities. Figure 5 shows temperature profiles based on single trajectory calculations with a fixed bath density of 324 kg/m<sup>3</sup> (283 atm) but varying the number of bath molecules as 69, 182, 400, and 1000 and varying the size of the box. It is seen that for 69 bath molecules the final system temperature at 100 ps is 460 K, whereas 1000 bath molecules approximately conserves the system temperature at

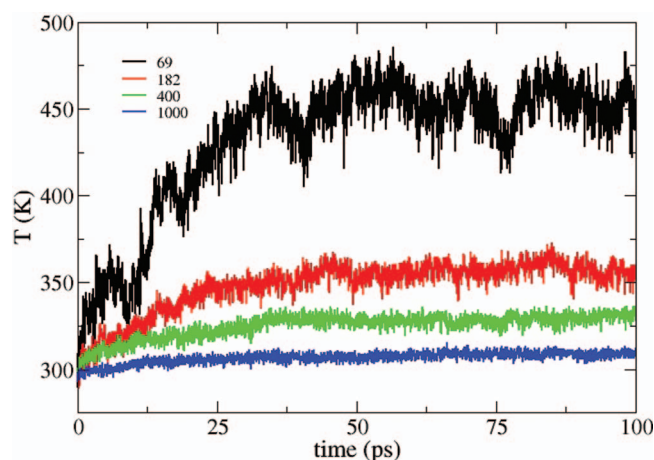


FIG. 5. Temperature profiles of single trajectory calculations, with different numbers of bath molecules, at a fixed bath density of 324 kg/m<sup>3</sup>. The density is kept constant by varying the size of the “simulation box.” The black, red, green, and blue curves are obtained from 69, 182, 400, and 1000 N<sub>2</sub> bath molecules, respectively.

310 K. Thus, for the 1000 molecules bath, during the simulation the system temperature remains within 5% of the initial 298 K temperature. If the bath density is changed by varying the number of solvent molecules, but keeping the same box size, there will be substantial heating of the bath at low density.

There is substantial interest in studying heating of the solvent bath, but for the work presented here the interest is in studying energy transfer to a bath which remains at the initial temperature. As discussed above, to a quite good approximation this is accomplished with a bath of 1000 N<sub>2</sub> molecules. The solvent systems for the current study were prepared in a cubic box with N<sub>2</sub> densities of 810, 324, 201, 80, and 40 kg/m<sup>3</sup>, for which the corresponding length of the box is 38.8, 52.6, 61.6, 83.7, and 105.4 Å, respectively. In order to obtain the desired density, the size of the box was varied keeping the number (1000) of bath molecules the same. The pressure for the highest and lowest densities, i.e., 810 and 40 kg/m<sup>3</sup>, are 707 and 35 atm at the 298 K simulation temperature.

Average energy transfer dynamics were obtained by calculating 96 trajectories for each density. To obtain the same final HFB energy from the simulations, for each N<sub>2</sub> density, it was necessary to run the trajectories for a longer time at the lower densities, i.e., there are fewer N<sub>2</sub> + C<sub>6</sub>F<sub>6</sub> collisions as the density is lowered. For the present study the simulation times are 312 ps for 40 kg/m<sup>3</sup>, 182 ps for 80 kg/m<sup>3</sup>, 133 ps for 201 kg/m<sup>3</sup>, 116 ps for 324 kg/m<sup>3</sup>, and 70 ps for 810 kg/m<sup>3</sup>, each with an integration time step of 0.006 ps. These times lead to a final total HFB energy of ~28 kcal/mol. This energy is slightly higher than the HFB average energy of 20.6 kcal/mol, which results if the initial 1886 kcal/mol total energy of HFB and the N<sub>2</sub> bath is statistically equilibrated between all the degrees of freedom. In addition to the HFB energy, the translational, rotational, and vibrational energies of the N<sub>2</sub> bath were also followed versus time.

## B. Analyses of the simulation results

As described in Sec. IV, for each density the average energy of HFB versus time  $\langle E(t) \rangle$ , is fit quite well by the bi-exponential expression

$$\langle E(t) \rangle = [E(0) - E(\infty)] \times [f_1 \exp(-k_1 t) + f_2 \exp(-k_2 t)] + E(\infty) \quad (7)$$

with  $f_1 + f_2 = 1$ ; i.e., see fittings and results given in the next section. As the solvent density is lowered, the energy transfer dynamics enters the independent, single collision limit where the energy transfer rate constant becomes proportional to pressure.

If  $\langle E(t) \rangle$  in Eq. (7) is differentiated with respect to the time, one obtains the average energy transfer per unit time for the value of  $\langle E(t) \rangle$ . If the independent single collision limit is considered and this  $d\langle E(t) \rangle/dt$  is divided by the number of collisions per unit time, i.e., the collision frequency  $\omega$ , one obtains the average energy transfer per collision, i.e.,

$$\langle \Delta E_c \rangle = [d\langle E(t) \rangle/dt] / \omega. \quad (8)$$

For a single exponential in Eq. (7) and for the  $t = 0$  limit, Eq. (8) becomes  $[E(0) - E(\infty)]k = -\langle \Delta E_c \rangle \omega$ , so that  $k$  is proportional to pressure (density), i.e.,

$$k = C \times \rho, \quad (9)$$

where  $k$  is the energy transfer rate constant,  $\rho$  is the density of the bath, and  $C$  is the proportionality constant and independent of  $\rho$  in the low density limit. For the current simulations, the first component of the bi-exponential dominates at short times and the independent single collision limit was determined by densities for which  $k_1$  is proportional to the density. However, as discussed in Sec. IV,  $k_2$  is found to be also proportional to the density in this limiting regime.

The collision frequency for each density is calculated using the formula

$$\omega = \pi \sigma^2 [M] \sqrt{\frac{8RT}{\pi \mu_{C_6F_6-N_2}}} \Omega_{2,2}^*, \quad (10)$$

which in convenient units may be written as<sup>100</sup>

$$\omega(s^{-1}) = 4.415 \times 10^7 \sigma^2 p (T\mu)^{-1/2} \Omega_{2,2}^*, \quad (11)$$

where  $[M]$  is the number density of the system,  $\sigma$  is the collision diameter in Å,  $p$  is the pressure (Torr),  $T$  is the temperature (K),  $\mu$  is in atomic mass units, and  $\Omega_{2,2}^*$  is collision integral taken as<sup>100</sup>

$$\Omega_{2,2}^* = \frac{A}{(T^*)^B} + \frac{C}{e^{DT^*}} + \frac{E}{e^{FT^*}}. \quad (12)$$

In Eq. (12),  $T^* = k_B T/\varepsilon$ , where  $k_B$  is the Boltzmann constant and  $\varepsilon$  is the intermolecular well depth, and the constants are  $A = 1.16145$ ,  $B = 0.14874$ ,  $C = 0.52487$ ,  $D = 0.77320$ ,  $E = 2.16178$ , and  $F = 2.43787$ .

Two approaches were used to determine the collision frequency. For the “experimental”  $\omega$  approach the values taken for  $\sigma$  and  $\varepsilon$  are 4.97 Å and 163 K, respectively, obtained from the relations  $\sigma = (\sigma_{C_6F_6} + \sigma_{N_2})/2$  and  $\varepsilon = \sqrt{\varepsilon_{C_6F_6} \varepsilon_{N_2}}$ , where the  $\sigma_{C_6F_6}$ ,  $\sigma_{N_2}$ ,  $\varepsilon_{C_6F_6}$ , and  $\varepsilon_{N_2}$  values are those used previously<sup>54</sup> to interpret experiments. For the *ab initio*  $\omega$  approach, two models were used to determine an average *ab initio* potential energy curve as discussed in Sec. II B 2 and shown in Figure 4. Figure 4(a) gives the orientation averaged N<sub>2</sub> + C<sub>6</sub>F<sub>6</sub> potential for which,  $\sigma = 5.12$  Å and  $\varepsilon = 250$  K. For the potential curve in Figure 4(b), each random orientation is Boltzmann weighted by its potential, and  $\sigma = 2.95$  Å and  $\varepsilon = 908$  K. One often considers a collision diameter, which equals  $\sigma$  times the square root of  $\Omega_{2,2}^*$ . The resulting experimental collision diameter is 5.47 Å and this collision diameter is 6.16 Å and 4.85 Å for the *ab initio* potential curves in Figures 4(a) and 4(b), respectively. The *ab initio* collision diameter for Figure 4(a) potential is larger than the experimental value as a result of the *ab initio*  $\varepsilon$  of 250 K as compared to the experimental  $\varepsilon$  of 163 K. For the *ab initio* potential in Figure 4(b) with Boltzmann weighting, including the collision integral  $\Omega_{2,2}^*$  significantly increases the collision diameter from 2.95 Å to 4.85 Å as a result of the potential’s large  $\varepsilon$  of 908 K.

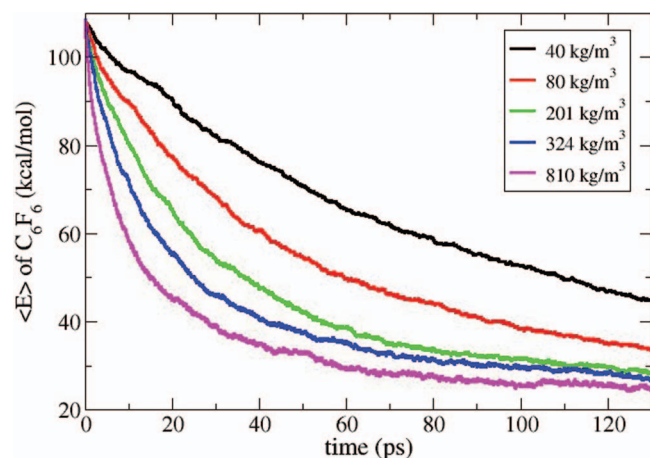


FIG. 6. Energy of HFB versus time, averaged over 96 trajectories, for  $N_2$  bath densities of 810, 324, 201, 80, and 40  $\text{kg/m}^3$ . There are 1000  $N_2$  molecules in the bath.

## IV. RESULTS AND DISCUSSION

### A. Energy transfer parameters and limiting density

In Figure 6, the average energy of HFB versus time,  $\langle E(t) \rangle$ , for 96 trajectories is presented for each of the densities. The  $\langle E(t) \rangle$  are excellently fit by Eq. (7), and the fitting parameters  $f_1, f_2, k_1, k_2$ , and  $E(\infty)$  are listed in Table III. For each density,  $\langle E(t) \rangle$  is highly non-exponential, with the weight of the large rate constant component apparently decreasing with decrease in density. Using  $k_i = C_i \rho$ , as shown in Eq. (9), the  $C_i$ 's for each density are also listed in Table III and are plotted versus density in Figure 7. The constants  $C_1$  and  $C_2$  become nearly independent of density between  $\rho$  of 80 and 40  $\text{kg/m}^3$  (particularly  $C_1$ ), and for the following analyses 40  $\text{kg/m}^3$  is taken to represent the independent, single collision limit. For this density, the “experimental” collision frequency is  $\omega = 0.41 \times 10^{12} \text{ s}^{-1}$  (see Sec. III B) and the mean free path for  $C_6F_6$  in  $N_2$  is 12.5 Å. For comparison with the latter, the experimental  $\sigma$  is 5.47 Å.

For the initial conditions “hot” HFB contains 107.4 kcal/mol vibrational energy, but only a 298 K Boltzmann distribution of rotational energy. It is of interest to determine if energy is transferred to HFB rotation as HFB is vibrationally relaxed. Analyses show that such HFB  $V \rightarrow R$  is unimportant. The average 298 K rotational energy of HFB is  $\sim 0.90$  kcal/mol and during the simulation the HFB rotational energy never becomes significantly larger than this value.

TABLE III. Parameters for fits to  $\langle E(t) \rangle$  for different bath densities.<sup>a</sup>

| $\rho$ ( $\text{kg/m}^3$ ) <sup>b</sup> | $E(\infty)$ | $f_1$ | $f_2$ | $k_1$  | $k_2$   | $C_1$    | $C_2$     |
|-----------------------------------------|-------------|-------|-------|--------|---------|----------|-----------|
| 40                                      | 22.2        | 0.256 | 0.744 | 0.0277 | 0.00810 | 0.000692 | 0.000202  |
| 80                                      | 25.5        | 0.279 | 0.730 | 0.0542 | 0.0154  | 0.000678 | 0.000192  |
| 201                                     | 27.2        | 0.278 | 0.722 | 0.0967 | 0.0274  | 0.000482 | 0.000136  |
| 324                                     | 27.4        | 0.388 | 0.612 | 0.149  | 0.0321  | 0.000460 | 0.0000987 |
| 810                                     | 26.6        | 0.458 | 0.542 | 0.291  | 0.0421  | 0.000360 | 0.0000519 |

<sup>a</sup>The fits are to Eq. (7). The sum of  $f_1$  and  $f_2$  is set to unity in the fitting, and the  $k$ 's are in unit of  $\text{ps}^{-1}$ .  $C_1$  and  $C_2$  are calculated by  $k_1/\rho$  and  $k_2/\rho$ , respectively (see Eq. (9)).

<sup>b</sup>The pressures for the lowest and highest densities of 40 and 810  $\text{kg/m}^3$  are 35 and 707 atm, respectively.

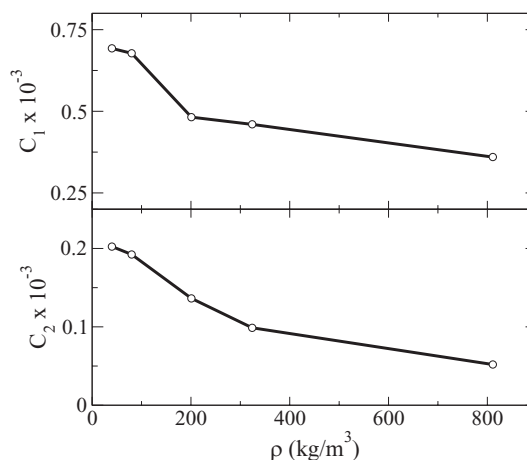


FIG. 7.  $C_1$  and  $C_2$  as computed from Eqs. (7) and (9) for the  $\langle E(t) \rangle$  of the different  $N_2$  bath densities in Figure 6.

Nevertheless, it is of interest that the small amount of  $V \rightarrow R$  for HFB depends on the  $N_2$  bath density. For the 810  $\text{kg/m}^3$  simulations  $\langle E_{rot} \rangle$  of HFB never exceeds 1.5 kcal/mol, while for the 201  $\text{kg/m}^3$  simulations  $\langle E_{rot} \rangle$  becomes as large as  $\sim 1.9$  kcal/mol within 0–10 ps time interval. For the 40  $\text{kg/m}^3$  simulations  $\langle E_{rot} \rangle$  becomes  $\sim 2.4$  kcal/mol at  $\sim 50$  ps and then decreases.

As discussed in Sec. III A, for each of the  $N_2$  bath densities the simulations were continued until the average total energy of HFB (i.e., translation, rotation, and vibration) attained a constant limiting value of  $\sim 28$  kcal/mol. This energy is slightly higher than the HFB average energy of 20.6 kcal/mol, which results if the initial total energy of the  $N_2$  bath and HFB molecule of 1886 kcal/mol is statistically equilibrated between all the  $N_2$  bath and HFB degrees of freedom. The resulting equilibrated  $N_2$  bath temperature is 314 K, consistent with the simulations as discussed in Sec. III A.

As shown in Table III, the fitted  $E(\infty)$  values vary from 22.2 kcal/mol for  $\rho = 40 \text{ kg/m}^3$  to 27.4 kcal/mol for  $\rho = 324 \text{ kg/m}^3$ . The former is only 1.6 kcal/mol larger than the value of 20.6 kcal/mol when the HFB/ $N_2$ -bath system becomes fully equilibrated at long time. If Eq. (7) was an exact representation of the HFB energy relaxation dynamics, the fitted  $E(\infty)$  values would equal 20.6 kcal/mol, and apparently Eq. (7) is the best representation of these dynamics for the lowest density simulations. That the fitted  $E(\infty)$  values are larger than the fully equilibrated value of 20.6 kcal/mol indicates that, in representing the long time decay of  $\langle E(t) \rangle$  to 20.6 kcal/mol, at least one additional exponential is required in Eq. (7) to fit The  $\langle E(t) \rangle$  to the  $t = \infty$  limit time. The need for additional exponentials and relaxation parameters in Eq. (7), to fit  $\langle E(t) \rangle$  for the complete time domain is considered in the summary.

### B. Energy transfer dynamics to the $N_2$ bath

The energy transfer from the vibrationally excited HFB molecule may be used to increase the translational, rotational, and vibrational energies of the  $N_2$  bath molecules. For each of the bath densities, within statistical uncertainties, there is

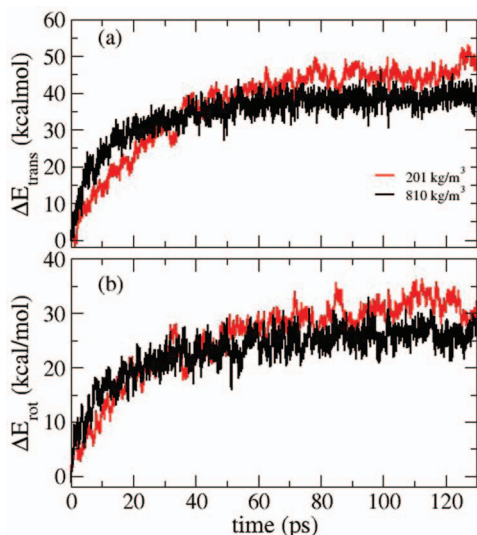


FIG. 8. The change in the total (a) translational and (b) rotational energies of the  $N_2$  bath, averaged over 96 trajectories. Results are illustrated for the bath densities of 201 and 810  $kg/m^3$ . There are 1000  $N_2$  molecules in the bath.

no energy transfer to  $N_2$  vibration during the simulations, and the vibrational energy transferred from HFB is used to increase the translational and rotational energies of the  $N_2$  molecules. This is illustrated in Figure 8 where the increase of the average translational and rotational energies of the  $N_2$  bath are plotted versus time (up to 130 ps) for the simulations with bath densities of 201 and 810  $kg/m^3$ . As discussed in Sec. III A, these respective simulations are integrated to 133 and 70 ps to attain the approximate “equilibrated” HFB energy of  $\sim 28$  kcal/mol. The final  $\langle E_{trans} \rangle$  is  $\sim 1.5$  times larger than  $\langle E_{rot} \rangle$  for each of the densities as expected for equilibration of the energy between  $N_2$  translation and rotation. In addition, there are no significant, discernible, statistical differences in the relative transfer of energy to  $N_2$  translation and rotation versus time.

### C. Average energy transfer per collision ( $\Delta E_c$ )

Using Eq. (8) and  $\langle E(t) \rangle$  in Figure 6 and the collision frequency  $\omega$ , the average energy transferred from HFB per collision as a function of  $\langle E \rangle$  may be determined. The resulting plot of  $\langle \Delta E_c \rangle$  versus  $\langle E \rangle$  is given in Figure 9(a) for each of the densities using the experimental collision frequency which includes the collision integral  $\Omega_{2,2}^*$  as discussed above in Sec. III B. Given in Figure 9(b) is the analogous  $\langle \Delta E_c \rangle$  versus  $\langle E \rangle$  plot for the orientation averaged *ab initio* potential without Boltzmann weighting. It is of interest that  $\langle \Delta E_c \rangle$  calculated in this manner increases for a fixed  $\langle E \rangle$  as the density approaches that for the independent, single collision limit. As expected from model analyses of experiments,<sup>32</sup>  $\langle \Delta E_c \rangle$  approaches zero as  $\langle E \rangle$  becomes small.  $\langle \Delta E_c \rangle$  is a composite of energy transfer from and to HFB, i.e.,  $\langle \Delta E_c^{down} \rangle$  and  $\langle \Delta E_c^{up} \rangle$ , respectively. At large  $\langle E \rangle$ ,  $\langle \Delta E_c^{down} \rangle$  dominates. At long times, when equilibrium is attained, the magnitudes of  $\langle \Delta E_c^{down} \rangle$  and  $\langle \Delta E_c^{up} \rangle$  become the same and  $\langle \Delta E_c \rangle$  equals zero.

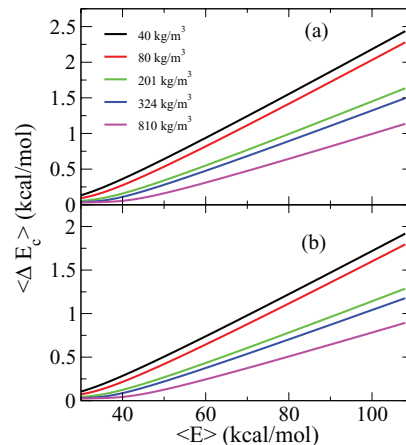


FIG. 9. Average energy transfer per collision for each  $N_2$  bath density using two sets of L-J parameters: (a) L-J parameters from the literature;<sup>54</sup> and (b) L-J parameters for the angle averaged  $C_6F_6-N_2$  interaction potential presented in the top graph of Figure 4.

From the discussion above, the  $\rho = 40$   $kg/m^3$  density simulation is a good representation of the single collision limit. For this density, the value of  $\langle \Delta E_c \rangle$  at  $\langle E \rangle = 85.8$  kcal/mol is 1.74 kcal/mol from Figure 9(a) which uses the experimental collision frequency<sup>54</sup> and in excellent agreement with the gas-phase experimental value of 1.60 kcal/mol.<sup>54</sup> From Figure 9(b), based on the orientation averaged *ab initio* potential  $\langle \Delta E_c \rangle$  is 1.37 kcal/mol for  $\langle E \rangle = 85.8$  kcal/mol. If Boltzmann-weighting is included with the orientation averaging, and the collision integral is included to determine the collision frequency (Sec. III B),  $\langle \Delta E_c \rangle$  becomes 2.14 kcal/mol at this  $\langle E \rangle$ .

It is of interest to consider which of the two approaches is more appropriate for determining the  $N_2 + C_6F_6$  average intermolecular potential energy curve (i.e., Figures 4(a) and 4(b)) and the resulting collision frequency. The approach without Boltzmann weighting is similar to that used in previous work by Bernshtein and Oref<sup>8</sup> and expected to be more representative of the actual collision dynamics. The Boltzmann weighting assumes thermal equilibrium, so that the collisions preferentially sample the strongest  $N_2 + C_6F_6$  attractive interactions. In contrast to such a model, the  $N_2 + C_6F_6$  collisions were direct without trapping and thermalization in the  $N_2 + C_6F_6$  potential energy minimum.

### D. Effect of $N_2-C_6F_6$ intermolecular potential

As discussed in Sec. II B 2, two analytic functions were fit for the  $N_2-C_6F_6$  intermolecular potential, PES1 and PES2. PES1 is fit to three  $N_2 + C_6F_6$  intermolecular potential energy curves, while PES2 is fit to four. PES2 is considered more accurate and was used for the simulations. However, the energy transfer dynamics, e.g.,  $\langle E(t) \rangle$  was found to be statistically the same for PES1 and PES2, and this is shown in Figure 10 for  $\rho = 324$   $kg/m^3$  simulation. Of interest is to determine the level of accuracy required for the  $N_2-C_6F_6$  intermolecular potential to obtain accurate energy transfer dynamics. This has been considered in previous collisional energy transfer studies<sup>101</sup> and it is a possible topic to investigate in future studies of

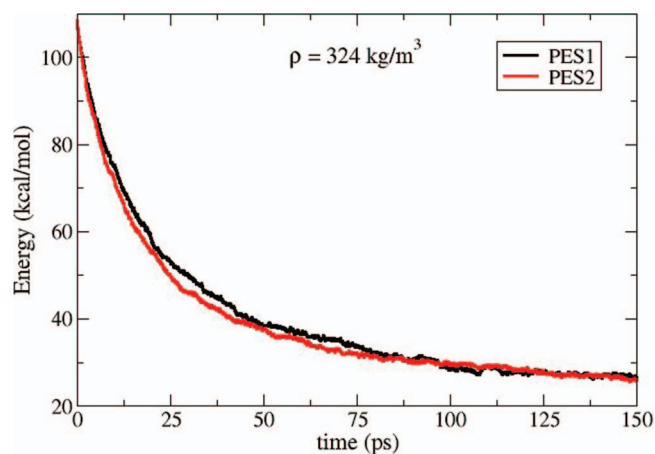


FIG. 10. Comparison of the energy of HFB versus time, averaged over 96 trajectories, for the PES1 and PES2 models of the  $C_6F_6-N_2$  intermolecular potential. Simulation results are for a  $N_2$  bath density of  $324 \text{ kg/m}^3$  and 1000 molecules in the bath.

$N_2 + C_6F_6$  collisions and related systems of collisional energy transfer.

### E. Analysis of the trajectory sample size

For the above simulations, 96 trajectories were calculated for each density to obtain average results. Of interest is whether meaningful results could be obtained with a smaller trajectory sample size. This was investigated for  $\rho = 40 \text{ kg/m}^3$  simulations. The 96 trajectories were split into two groups of 48 each and into four groups of 24 each. For each group the average energy of HFB versus time,  $\langle E(t) \rangle$ , was calculated. The resulting plots are shown in Figure 11, when they are compared with each other and with the plot for the 96 trajectories. To quantitatively access the differences in the  $\langle E(t) \rangle$  each was fit with the bi-exponential in Eq. (7), and the results are given in Table IV. For the two groups of 48 trajectories, the fitted parameters are similar to the values for 96 trajectory ensemble. The four groups, of 24 trajectories

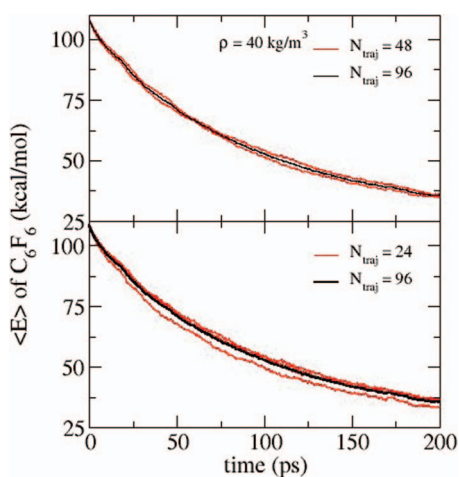


FIG. 11. Average energy of HFB versus time, averaged over: 96 trajectories (black); two ensembles of 48 trajectories; and four ensembles of 24 trajectories. Results are for a  $N_2$  bath density of  $40 \text{ kg/m}^3$  and 1000 molecules in the bath.

TABLE IV. Parameters for fits to  $\langle E(t) \rangle$  for different simulation ensemble sizes.<sup>a</sup>

| No. Trajs. <sup>b</sup> | $E(\infty)$ | $f_1$ | $f_2$ | $k_1$  | $k_2$   |
|-------------------------|-------------|-------|-------|--------|---------|
| 96                      | 22.2        | 0.256 | 0.744 | 0.0277 | 0.00810 |
| 48                      | 24.1        | 0.253 | 0.747 | 0.0260 | 0.00854 |
| 48                      | 23.1        | 0.279 | 0.721 | 0.0283 | 0.00869 |
| 24                      | 21.2        | 0.240 | 0.760 | 0.0270 | 0.00802 |
| 24                      | 27.4        | 0.230 | 0.770 | 0.0258 | 0.00959 |
| 24                      | 26.1        | 0.201 | 0.799 | 0.0278 | 0.00955 |
| 24                      | 21.4        | 0.296 | 0.704 | 0.0288 | 0.00877 |

<sup>a</sup>The simulations are for the  $40 \text{ kg/m}^3$  density. The fits are to Eq. (7). The sum of  $f_1$  and  $f_2$  is set to unity in the fitting, and the  $k$ 's are in unit of  $\text{ps}^{-1}$ .

<sup>b</sup>The results for the 96 trajectory ensemble are from Table III. For the 48 and 24 trajectory ensembles, the 96 trajectory ensemble is split into two and four groups, respectively.

each, show more variability in the fitted parameters, but overall they display the same energy transfer dynamics and each give semi-quantitative results. This analysis indicates that, for the simulation model used here, meaningful intermolecular energy transfer dynamics may be obtained with a relatively small sample size. The most likely reason for this finding is the extensive averaging resulting from the collisions of HFB with the  $N_2$  bath. In a traditional trajectory simulation of intermolecular energy transfer, collisions are considered between the vibrationally excited molecules and a single bath model.<sup>10–16</sup> A large ensemble of trajectories is then required to obtain a meaningful average over random initial conditions for the collision partners.

### V. SUMMARY

In this work, molecular dynamics simulations are reported for the study of collisional energy transfer dynamics for a highly excited HFB molecule in a  $N_2$  bath. The simulations are performed with one HFB molecule in a periodic “box” of  $N_2$  molecules. By varying the size of the box and/or number of  $N_2$  molecules, the simulation may be performed for either the liquid or gas phase. Electronic structure calculations were performed at the MP2/aug-cc-pVTZ level of theory to determine  $N_2-N_2$  and  $N_2-C_6F_6$  intermolecular potentials for the simulations, which were represented by sums of two-body potentials. The  $N_2 + C_6F_6$  collisional energy transfer dynamics were found to be insensitive to fine details of the  $N_2-C_6F_6$  intermolecular potential.

The extent of heating of the bath, as HFB relaxes, is determined by the number of  $N_2$  molecules in the bath. For a simulation to compare with experiment, with “hot” HFB initially containing 107.4 kcal/mol of vibrational energy, the temperature is preserved within 5% of the 298 K initial temperature with a bath of 1000  $N_2$  molecules. For the  $\sim 100$ – $300$  ps simulations and all bath densities, energy transfer from HFB is to  $N_2$  rotation and translation with no energy transfer to  $N_2$  vibration. In addition, there is negligible transfer of energy from HFB vibration to HFB rotation. Apparently, the simulations could be performed with the  $N_2$  vibration “frozen” and removed from the simulation degrees of freedom.

For all densities the average total energy of HFB as a function of time from the simulations,  $\langle E(t) \rangle$ , is accurately fit by the bi-exponential expression in Eq. (7), with the long-time equilibrated energy  $E(\infty)$  treated as a fitting parameter. At a density of 40 kg/m<sup>3</sup>, the simulation system attains the single collision gas-phase model and the collisional deactivation rate constant is directly proportional to the density. In this collision limit, the average energy transferred per unit time,  $d[\langle E(t) \rangle]/dt$ , may be divided by the collision frequency  $\omega$  to obtain the average energy transferred per collision  $\langle \Delta E_c \rangle$ . With the collision frequency used to interpret experiments, the resulting  $\langle \Delta E_c \rangle$  is 1.74 kcal/mol at  $\langle E \rangle = 85.8$  kcal/mol and in excellent agreement with experiment.<sup>54</sup>

The simulations were extended for  $\sim 100$ – $300$  ps and until  $\langle E(t) \rangle$  was  $\sim 28$  kcal/mol, which is higher than the fully equilibrated HFB energy of 20.6 kcal/mol. The fitted  $E(\infty)$  values for the simulations, listed in Table III, are larger than this long time, fully equilibrated value. For a complete representation of  $\langle E(t) \rangle$ , extended to long times, an additional exponential(s) will be needed for Eq. (7) with a smaller relaxation rate constant(s). The time required to attain a fully equilibrated HFB molecule in the N<sub>2</sub> bath is an interesting and important question. A related issue is equilibration of the N<sub>2</sub> translational, rotational, and vibrational energies. No energy is transferred to N<sub>2</sub> vibration as HFB is relaxed during the simulations, and equilibration of N<sub>2</sub> vibration with N<sub>2</sub> rotation and translation is expected to occur on a much longer time scale than that for the  $\sim 100$ – $300$  ps simulations.

For the current study there is only a well defined, single HFB energy at the beginning of the simulation; i.e., 107.4 kcal/mol. As HFB relaxes within the N<sub>2</sub> bath, it acquires a distribution of energy, whose average is  $\langle E(t) \rangle$ . Thus, for each time, the energy transfer and  $\langle \Delta E_c \rangle$  is for an energy distribution, which contrasts with previous studies<sup>8, 16, 103–105</sup> for which  $\langle \Delta E_c \rangle$  was determined for fixed energies. It is of interest that for the current study no more than 96 trajectories are required to study energy transfer for this distribution as it evolves in time. In previous work,<sup>15, 102–106</sup> Schatz and co-workers<sup>16</sup> have performed somewhat similar simulations of ensemble-averaged intermolecular energy transfer.

For the decay of  $\langle E(t) \rangle$ , the slope  $d[\langle E(t) \rangle]/dt$  decreases with decrease in  $\langle E(t) \rangle$ , and the corresponding value of  $\langle \Delta E_c \rangle$  also decreases. Thus, energy transfer from HFB is predicted to become less efficient as  $\langle E(t) \rangle$  is lowered. Such an effect has been observed for relaxation of pyrazine, where changing the pyrazine internal energy by 7%, from 37 900 to 40 600 cm<sup>-1</sup>, changes the energy transfer probability by a factor of 3.<sup>42</sup> A strong energy dependence for  $\langle \Delta E_c \rangle$  was also found in fixed energy simulations by Schatz and co-workers<sup>16, 103–105</sup> and Bernshtein and Oref,<sup>8</sup> and also in ensemble average simulations by Schatz and co-workers.<sup>15, 102–106</sup> An increased vibrational density of states is expected to increase the efficiency of energy transfer,<sup>47</sup> which is consistent with a decrease in  $\langle \Delta E_c \rangle$  as  $\langle E(t) \rangle$  is lowered and the density is decreased. At very low  $\langle E(t) \rangle$  energy transfer is expected to become quite inefficient and, with the low state density, may become vibrational state dependent. An interesting question is if there is an approximate high energy limiting value of  $\langle \Delta E_c \rangle$ . For the current study, where  $\langle \Delta E_c \rangle$  corresponds to a distribution of HFB

energies, the role of the HFB density of states on the energy transfer will involve a convolution of  $\Delta E_c$  for the different HFB energies in the distribution.

In future work, it will be possible to calculate  $\langle E(t) \rangle$  and the corresponding  $\langle \Delta E_c \rangle$  for a series of energized and bath molecules, and relate the efficiency of collisional energy transfer to the energized molecules' densities of states and properties of the deactivating bath molecules and their intermolecular potentials with the energized molecules.

## ACKNOWLEDGMENTS

The research reported here is based upon work supported by the Air Force Office of Scientific Research (AFOSR) BRI Grant No. FA 9550-12-1-0443, and the Robert A. Welch Foundation under Grant No. D-0005. Support was also provided by the High Performance Computing Center (HPCC) at Texas Tech University, under the direction of Philip W. Smith. Parts of the computation are also done on Robinson, a general computer cluster of Department of Chemistry and Biochemistry, Texas Tech University, purchased by the NSF CRIF-MU Grant No. CHE-0840493.

- <sup>1</sup>D. C. Tardy and B. S. Rabinovitch, *Chem. Rev.* **77**, 369 (1977).
- <sup>2</sup>M. Quack and J. Troe, *Gas Kinetics and Energy Transfer* (The Chemical Society, London, 1977), Vol. 2.
- <sup>3</sup>H. Hippler and J. Troe, in *Biomolecular Collisions*, edited by M. N. R. Ashfold and J. E. Baggott (Royal Society of Chemistry, London, 1989).
- <sup>4</sup>I. Oref and D. C. Tardy, *Chem. Rev.* **90**, 1407 (1990).
- <sup>5</sup>J. R. Barker and B. M. Toselli, *Int. Rev. Phys. Chem.* **12**, 305 (1993).
- <sup>6</sup>G. W. Flynn, C. S. Parmenter, and A. M. Wodtke, *J. Phys. Chem.* **100**, 12817 (1996).
- <sup>7</sup>V. Bernshtein, I. Oref, and G. Lendvay, *J. Phys. Chem.* **100**, 9738 (1996).
- <sup>8</sup>V. Bernshtein and I. Oref, *J. Chem. Phys.* **108**, 3543 (1998).
- <sup>9</sup>R. G. Gilbert, *J. Chem. Phys.* **80**, 5501 (1984).
- <sup>10</sup>N. Date, W. L. Hase, and R. G. Gilbert, *J. Phys. Chem.* **88**, 5135 (1984).
- <sup>11</sup>W. L. Hase, N. Date, L. B. Bhuiyan, and D. G. Buckowski, *J. Phys. Chem.* **89**, 2502 (1985).
- <sup>12</sup>X. Hu and W. L. Hase, *J. Phys. Chem.* **92**, 4040 (1988).
- <sup>13</sup>A. R. Whyte, K. F. Lim, R. G. Gilbert, and W. L. Hase, *Chem. Phys. Lett.* **152**, 377 (1988).
- <sup>14</sup>N. J. Brown and J. A. Miller, *J. Chem. Phys.* **80**, 5568 (1984).
- <sup>15</sup>M. Bruehl and G. C. Schatz, *J. Chem. Phys.* **92**, 6561 (1990).
- <sup>16</sup>G. Lendvay and G. C. Schatz, *J. Chem. Phys.* **96**, 4356 (1992).
- <sup>17</sup>M. L. Strekalov, *Chem. Phys. Lett.* **431**, 1 (2006).
- <sup>18</sup>R. A. Bustos-Marín, E. A. Coronado, and J. C. Ferrero, *J. Chem. Phys.* **127**, 154305 (2007).
- <sup>19</sup>R. G. Gilbert, *Aust. J. Chem.* **48**, 1787 (1995).
- <sup>20</sup>T. Lenzer, K. Luther, J. Troe, R. G. Gilbert, and K. F. Lim, *J. Chem. Phys.* **103**, 626 (1995).
- <sup>21</sup>T. Lenzer and K. Luther, *J. Chem. Phys.* **105**, 10944 (1996).
- <sup>22</sup>V. Bernshtein and I. Oref, *J. Chem. Phys.* **106**, 7080 (1997).
- <sup>23</sup>S. H. Kable and A. E. W. Knight, *J. Phys. Chem. A* **107**, 10813 (2003).
- <sup>24</sup>K. F. Lim, *J. Chem. Phys.* **100**, 7385 (1994).
- <sup>25</sup>V. Bernshtein and I. Oref, *J. Chem. Phys.* **104**, 1958 (1996).
- <sup>26</sup>K. F. Lim and R. G. Gilbert, *J. Chem. Phys.* **84**, 6129 (1986).
- <sup>27</sup>K. F. Lim and R. G. Gilbert, *J. Chem. Phys.* **92**, 1819 (1990).
- <sup>28</sup>D. L. Clarke, I. Oref, R. G. Gilbert, and K. F. Lim, *J. Chem. Phys.* **96**, 5983 (1992).
- <sup>29</sup>D. L. Clarke and R. G. Gilbert, *J. Phys. Chem.* **96**, 8450 (1992).
- <sup>30</sup>C. Heidelbach, I. I. Fedchenia, D. Schwarzer, and J. Schroeder, *J. Chem. Phys.* **108**, 10152 (1998).
- <sup>31</sup>C. Heidelbach, V. S. Vikhrenko, D. Schwarzer, and J. Schroeder, *J. Chem. Phys.* **110**, 5286 (1999).
- <sup>32</sup>M. J. Rossi, J. R. Pladziewicz, and J. R. Barker, *J. Chem. Phys.* **78**, 6695 (1983).
- <sup>33</sup>M. L. Yerram, J. D. Brenner, K. D. King, and J. R. Barker, *J. Phys. Chem.* **94**, 6341 (1990).

- <sup>34</sup>B. M. Toselli and J. R. Barker, *Chem. Phys. Lett.* **174**, 304 (1990).
- <sup>35</sup>B. M. Toselli, J. D. Brenner, M. L. Yerram, W. E. Chin, K. D. King, and J. R. Barker, *J. Chem. Phys.* **95**, 176 (1991).
- <sup>36</sup>B. M. Toselli and J. R. Barker, *J. Chem. Phys.* **95**, 8108 (1991).
- <sup>37</sup>B. M. Toselli and J. R. Barker, *J. Chem. Phys.* **97**, 1809 (1992).
- <sup>38</sup>J. R. Barker, L. M. Yoder, and K. D. King, *J. Phys. Chem. A* **105**, 796 (2001).
- <sup>39</sup>C. A. Michaels, A. S. Mullin, and G. W. Flynn, *J. Chem. Phys.* **102**, 6682 (1995).
- <sup>40</sup>C. A. Michaels, Z. Lin, A. S. Mullin, H. C. Tapalian, and G. W. Flynn, *J. Chem. Phys.* **106**, 7055 (1997).
- <sup>41</sup>M. C. Wall, B. A. Stewart, and A. S. Mullin, *J. Chem. Phys.* **108**, 6185 (1998).
- <sup>42</sup>M. C. Wall and A. S. Mullin, *J. Chem. Phys.* **108**, 9658 (1998).
- <sup>43</sup>M. Fraelich, M. S. Elioff, and A. S. Mullin, *J. Phys. Chem. A* **102**, 9761 (1998).
- <sup>44</sup>M. C. Wall, A. S. Lemoff, and A. S. Mullin, *J. Phys. Chem. A* **102**, 9101 (1998).
- <sup>45</sup>M. S. Elioff, M. C. Wall, A. S. Lemoff, and A. S. Mullin, *J. Chem. Phys.* **110**, 5578 (1999).
- <sup>46</sup>D. K. Havey, Q. Liu, Z. Li, M. Elioff, M. Fang, J. Neudel, and A. S. Mullin, *J. Phys. Chem. A* **111**, 2458 (2007).
- <sup>47</sup>L. Yuan, J. Du, and A. S. Mullin, *J. Chem. Phys.* **129**, 014303 (2008).
- <sup>48</sup>J. Du, L. Yuan, S. Hsieh, F. Lin, and A. S. Mullin, *J. Phys. Chem. A* **112**, 9396 (2008).
- <sup>49</sup>Q. Liu, D. K. Havey, and A. S. Mullin, *J. Phys. Chem. A* **112**, 9509 (2008).
- <sup>50</sup>A. J. Sedlacek, R. E. Weston, Jr., and G. W. Flynn, *J. Chem. Phys.* **94**, 6483 (1991).
- <sup>51</sup>C. A. Michaels and G. W. Flynn, *J. Chem. Phys.* **106**, 3558 (1997).
- <sup>52</sup>D. G. Mitchell, A. M. Johnson, J. A. Johnson, K. A. Judd, K. Kim, M. Mayhew, A. L. Powell, and E. T. Sevy, *J. Phys. Chem. A* **112**, 1157 (2008).
- <sup>53</sup>H. Hippler, J. Troe, and H. J. Weldenken, *J. Chem. Phys.* **78**, 5351 (1983); **78**, 6709 (1983); **78**, 6718 (1983); **80**, 1853 (1984).
- <sup>54</sup>M. Dumm, H. Hippler, H. A. Olschewski, J. Troe, and J. Willner, *Z. Phys. Chem. N. F.* **166**, 129 (1990).
- <sup>55</sup>H. Hippler, J. Troe, and H. J. Weldenken, *Chem. Phys. Lett.* **84**, 257 (1981).
- <sup>56</sup>N. Nakashima and K. Yoshihara, *J. Chem. Phys.* **79**, 2727 (1983).
- <sup>57</sup>T. Ichimura, M. Takahashi, and Y. Mori, *Chem. Phys.* **114**, 111 (1987).
- <sup>58</sup>T. Ichimura, Y. Mori, N. Nakashima, and K. Yoshihara, *J. Chem. Phys.* **83**, 117 (1985).
- <sup>59</sup>T. Ichimura, Y. Mori, N. Nakashima, and K. Yoshihara, *Chem. Phys. Lett.* **104**, 533 (1984).
- <sup>60</sup>C.-L. Liu, H.-C. Hsu, J.-J. Lyu, and C.-K. Ni, *J. Chem. Phys.* **124**, 054302 (2006).
- <sup>61</sup>C.-L. Liu, H.-C. Hsu, Y. C. Hsu, and C.-K. Ni, *J. Chem. Phys.* **127**, 104311 (2007).
- <sup>62</sup>C.-L. Liu, H.-C. Hsu, Y. C. Hsu, and C.-K. Ni, *J. Chem. Phys.* **128**, 124320 (2008).
- <sup>63</sup>C.-L. Liu, H.-C. Hsu, and C.-K. Ni, *J. Chem. Phys.* **128**, 164316 (2008).
- <sup>64</sup>H.-C. Hsu, M.-T. Tsai, Y. A. Dyakov, and C.-K. Ni, *J. Chem. Phys.* **135**, 054311 (2011).
- <sup>65</sup>H.-C. Hsu, C.-L. Liu, Y. C. Hsu, and C.-K. Ni, *J. Chem. Phys.* **129**, 044301 (2008).
- <sup>66</sup>H. G. Loehmannsroeben and K. Luther, *Chem. Phys. Lett.* **144**, 473 (1988).
- <sup>67</sup>U. Grigoleit, T. Lenzer, K. Luther, M. Muetzer, and A. Takahara, *Phys. Chem. Chem. Phys.* **3**, 2191 (2001).
- <sup>68</sup>E. R. Waclawik, W. D. Lawrance, and R. A. J. Borg, *J. Phys. Chem.* **97**, 5798 (1993).
- <sup>69</sup>R. A. J. Borg, E. R. Waclawik, Mudjijono, and W. D. Lawrance, *Chem. Phys. Lett.* **218**, 320 (1994).
- <sup>70</sup>T. C. Brown, K. D. King, J.-M. Zellweger, and J. R. Barker, *Ber. Bunsen-Ges. Phys. Chem.* **89**, 301 (1985).
- <sup>71</sup>J.-M. Zellweger, T. C. Brown, and J. R. Barker, *J. Chem. Phys.* **83**, 6251 (1985).
- <sup>72</sup>J. R. Gascooke, Z. T. Alwahabi, K. D. King, and W. D. Lawrance, *J. Phys. Chem. A* **102**, 8505 (1998).
- <sup>73</sup>R. M. Whitnell, K. R. Wilson, and J. T. Hynes, *J. Phys. Chem.* **94**, 8625 (1990).
- <sup>74</sup>R. M. Whitnell, K. R. Wilson, and J. T. Hynes, *J. Chem. Phys.* **96**, 5354 (1992).
- <sup>75</sup>P. Valentini and T. E. Schwartzentruber, *Phys. Fluids* **21**, 066101 (2009).
- <sup>76</sup>P. Valentini and T. E. Schwartzentruber, *J. Comput. Phys.* **228**, 8766 (2009).
- <sup>77</sup>P. Valentini, C. Zhang, and T. E. Schwartzentruber, *Phys. Fluids* **24**, 106101 (2012).
- <sup>78</sup>P. Norman, P. Valentini, and T. E. Schwartzentruber, *J. Comput. Phys.* **247**, 153 (2013).
- <sup>79</sup>P. Valentini, P. A. Tump, C. Zhang, and T. E. Schwartzentruber, *J. Thermophys. Heat Transfer* **27**, 226 (2013).
- <sup>80</sup>A. V. George, L. D. Field, and T. W. Hambley, *The Essentials of Organic Chemistry* (Prentice Hall, 1996).
- <sup>81</sup>D. Caraiman, G. K. Koyanagi, and D. K. Bohme, *J. Phys. Chem. A* **108**, 978 (2004).
- <sup>82</sup>V. Laporta, R. Celiberto, and J. M. Wadehra, *Plasma Sources Sci. Technol.* **21**, 055018 (2012).
- <sup>83</sup>M. Valiev, E. J. Bylaska, N. Govind, K. Kowalski, T. P. Straatsma, H. J. J. van Dam, D. Wang, J. Nieplocha, E. Apra, T. L. Windus, and W. A. de Jong, *Comput. Phys. Commun.* **181**, 1477 (2010).
- <sup>84</sup>C. Möller and M. S. Plesset, *Phys. Rev.* **46**, 618 (1934).
- <sup>85</sup>S. Simon, M. Duran, and J. J. J. Dannenberg, *Chem. Phys.* **105**, 11024 (1996).
- <sup>86</sup>K. E. Riley and P. Hobza, *J. Phys. Chem. A* **111**, 8257 (2007).
- <sup>87</sup>G. Vayner, Y. Alexeev, J. Wang, T. L. Windus, and W. L. Hase, *J. Phys. Chem. A* **110**, 3174 (2006).
- <sup>88</sup>U. Tasić, Y. Alexeev, G. Vayner, T. D. Crawford, T. L. Windus, and W. L. Hase, *Phys. Chem. Chem. Phys.* **8**, 4678 (2006).
- <sup>89</sup>S. Krukowski and P. Strak, *J. Chem. Phys.* **124**, 134501 (2006).
- <sup>90</sup>P. Strak and S. Krukowski, *J. Chem. Phys.* **126**, 194501 (2007).
- <sup>91</sup>K. A. Peterson, D. E. Woon, and T. H. Dunning, Jr., *J. Chem. Phys.* **100**, 7410 (1994).
- <sup>92</sup>J. M. C. Marques, F. V. Prudente, F. B. Pereira, M. M. Almeida, A. M. Maniero, and C. E. Fellows, *J. Phys. B: At. Mol. Opt. Phys.* **41**, 085103 (2008).
- <sup>93</sup>J. Wang and W. L. Hase, *J. Phys. Chem. B* **109**, 8320 (2005).
- <sup>94</sup>G. H. Peslherbe, H. Wang, and W. L. Hase, *Adv. Chem. Phys.* **105**, 171 (1999).
- <sup>95</sup>J. O. Hirschfelder, C. F. Curtiss, and R. B. Bird, *The Molecular Theory of Gases and Liquids* (John Wiley & Sons, Inc., New York, 1954).
- <sup>96</sup>W. L. Hase and D. G. Buckowski, *Chem. Phys. Lett.* **74**, 284 (1980).
- <sup>97</sup>W. L. Hase *et al.*, "VENUS96: A general chemical dynamics computer program," *QCPE Bull.* **16**, 671 (1996).
- <sup>98</sup>M. P. Allen and D. J. Tildesley, *Computer Simulation of Liquids* (Clarendon, Oxford, 1996).
- <sup>99</sup>Y. L. Yarnell, M. J. Katz, R. G. Wenzel, and S. H. Koenig, *Phys. Rev. A* **7**, 2130 (1973).
- <sup>100</sup>R. G. Gilbert and S. C. Smith, *Theory of Unimolecular and Recombination Reactions* (Blackwell Scientific Publication, 1990).
- <sup>101</sup>O. Meroueh and W. L. Hase, *J. Phys. Chem. A* **103**, 3981 (1999).
- <sup>102</sup>M. Bruehl and G. C. Schatz, *J. Chem. Phys.* **89**, 770 (1988).
- <sup>103</sup>M. Bruehl and G. C. Schatz, *J. Phys. Chem.* **92**, 7223 (1988).
- <sup>104</sup>G. Lendvay and G. C. Schatz, *J. Phys. Chem.* **95**, 8748 (1991).
- <sup>105</sup>G. Lendvay and G. C. Schatz, *J. Chem. Phys.* **98**, 1034 (1993).
- <sup>106</sup>G. C. Schatz and G. Lendvay, *J. Chem. Phys.* **106**, 3548 (1997).